




Modeling of heat transfer performance of carbon nanotube nanofluid in a tube with fixed wall temperature by using ANN–GA

Fatemeh Nasirzadehroshenin¹, Milad Sadeghzadeh², Amirhossein Khadang³, Heydar Maddah², Mohammad Hossein Ahmadi^{4,a}, Hossein Sakhaeinia⁵, Lingen Chen^{6,b} 

¹ Department of Chemistry, Islamic Azad University Central Tehran (IAUCT), Tehran, Iran

² Department of Renewable Energy and Environmental Engineering, University of Tehran, Tehran, Iran

³ Department of Chemistry, Payame Noor University (PNU), P.O.Box 19395-3697, Tehran, Iran

⁴ Faculty of Mechanical Engineering, Shahrood University of Technology, Shahrood, Iran

⁵ Department of Chemical Engineering, Central Tehran Branch, Islamic Azad University, Tehran, Iran

⁶ Institute of Thermal Science and Power Engineering, Wuhan Institute of Technology, Wuhan 430205, China

Received: 12 September 2019 / Accepted: 12 January 2020 / Published online: 3 February 2020

© Società Italiana di Fisica (SIF) and Springer-Verlag GmbH Germany, part of Springer Nature 2020

Abstract In this research, the heat transfer performance of carbon nanotube (CNT)/water nanofluid in a horizontal tube with a fixed wall temperature with a turbulent regime flow condition is experimentally analyzed. The heat transfer performance is monitored through an evaluation of the heat transfer coefficient and friction factor. To perform this investigation, the affecting performance variables of nanofluid such as volume concentration, twist ratio, and Reynolds number are defined and considered within certain ranges of 0.2–1.2%, 2–8, and 4000–20,000, respectively. It is monitored that insertion of nanoparticles of CNT increases the heat transfer coefficient in comparison with the water and its value is also boosted in higher concentrations and Reynolds number. It is found that simultaneous utilization of nanofluids and twisted tape influences the heat transfer more efficient than employing either nanofluid or twisted tape, individually. In overall, under the designed circumstances, the highest thermal performance factor is obtained at CNT concentration of 1.2% and twist ratio of 2.

List of symbols

ANN	Artificial neural network
Bf	Base fluid
BP	Back propagation
C_p	Specific heat
CNT	Carbon nanotube
d_i	Diameter
E	Enhanced case
f	Friction factor

^a e-mails: mohammadhosein.ahmadi@gmail.com; mhosein.ahmadi@shahroodut.ac.ir

^b e-mails: lingenchen@hotmail.com; lgchenna@yahoo.com

GA	Genetic algorithm
k	Thermal conductivity
MSE	Mean squared error
N	Number of data
NE	Not enhanced case
Nu	Nusselt number
nf	Nanofluid
Pr	Prandtl number
R^2	R -squared
Re	Reynolds number
RMSE	Root mean squared error
sim	Simulation
SVR	Support vector machine
TR	Twist ratio
\dot{V}	Volumetric flow
w	Width
y	Height
ρ	Density
\emptyset	Volume concentration
μ	Dynamic viscosity
δ	Thickness
ΔP	Pressure drop

1 Introduction

Passive enhancement methods are currently considered as appropriate approaches to increase the heat transfer rate without any requirement to an external force [1, 2]. These methods consist of surface coating, utilization of rough surfaces, insertion of additional liquids such as nanoparticles, turbulence makers, and generation of swirl–vortex through designing of twisted tapes, helical screw tapes, snail entrances, and tangential inlet nozzles [3, 4]. Among the mentioned passive techniques, utilization of twisted tapes and insertion of nanofluids attract more attentions to be used in the heat exchangers in order to improve the thermal performance [5]. Numerous advantages have been counted for these two techniques so far such as larger relative surface area, better heat conduction, acceptable stability, least clogging, and the establishment of a swirling flow and augmentation of the turbulence intensity near to the tube wall [6, 7]. Various researches have been carried out to boost the heat transfer rate through the utilization of nanofluid [8, 9] and twisted tapes [10].

The nanofluid is a suspension of solid in typical working fluids such as water, ethylene glycol, and engine oil [11]. The most attractive characteristic of nanofluid is its improved heat transfer performances including higher thermal conductivity and larger convective heat transfer coefficient compared with the base fluid, while the chemical and physical specifications of the base fluid are not changed significantly after insertion of nanofluids [12, 13]. This extensive intensification in heat transfer will result in decreasing energy cost, making smaller the equipment's size, and improving the effectiveness of the system [14]. The application of insertion nano-sized particles in typical fluids was firstly investigated by Eastman et al. [15] and verified the enhancement in the thermal conductivity of nanofluids. Eastman et al. [15] performed an investigation which is highly followed by other scientists in this field. The authors reported that applying copper nanoparticles in the ethylene glycol at a volume

concentration of 0.3% improved the thermal conductivity around 40% in comparison with the simple base fluid. Followed by Eastman, several reviews and researches have reported that nanofluids are able to enhance the thermal conductivity [16, 17]. Wen and Ding [18] analyzed the performance of Al_2O_3 /water nanofluid in a simple copper tube under a laminar flow. It was found that the improvement was considerable in the inlet of the tube. Yang et al. [19] experimented the influence of using nanofluids in a horizontal tube heat exchanger under laminar flow. Various nanofluids were considered, and it is found that the graphite nanoparticles have this feature to significantly increase the convective heat transfer coefficient at low weight concentrations. Hwang et al. [20] calculated the pressure drop and convective heat transfer coefficient of Al_2O_3 /water nanofluid in an experiment by providing a fully developed laminar flow condition in a circular tube which was heated steadily. It was monitored that utilization of nanofluid at a volume concentration of 0.3% enhanced the convective heat transfer coefficient by 8% in comparison with the simple base fluid. Xie et al. [21] experimented the effects of applying ZnO, Al_2O_3 , MgO, and TiO_2 in a hybrid base fluid (55% DI water–45% ethylene glycol) at a circular tube heat exchanger at laminar flow condition with a fixed wall temperature on the convective heat transfer coefficient. It was monitored that features including the size of the nanoparticles, the number of suspended nanoparticles, and flow regime were highly influential on the thermal performance. In other words, these parameters have increased the viscosity of the nanofluids. Augmentation of the thermal conductivity of nanofluid is not individually sufficient for obtaining an ideally improved heat transfer rate in the heat exchangers. Therefore, additional researches are essential in this topic.

As mentioned above, utilization of twisted tape is a passive technique which is highly favorable in the applications of heat exchangers. Twisted tape is mainly used due to the ability to generate the swirl flow without imposing any considerable expenses and can be easily used in an existing heat exchanger. Various numerical and experimental researches have been carried out so far to assess the influence of employing the twisted tape. Twisted tape insertion causes redeveloping the thermal boundary layer and generating swirl flow, totally improving the convective heat transfer coefficient. Twisted tape is an appropriate selection for upgrading available compact heat exchangers due to its simple installation procedure, uncomplicated maintenance instructions, and majorly its cheapness. In addition to its positive effects, insertion of twisted tapes also increases the friction loss in the system [22]. In order to overcome this generated friction loss, more pumping power is required which has an influence on the performance factor, and increases the pumping cost. Hence, to obtain a favorable heat transfer rate in addition to a cost-effective pumping work, a special layout of twisted tape with an appropriate geometry and shape is demanded.

Several investigations have been performed to evaluate the influences of applying twisted tapes [23, 24]. Positive effects of nanofluids and twisted tapes on the improvement in heat transfer rate encourage researchers to investigate these applications, simultaneously [25, 26]. Mahyari et al. [27] performed an experimental investigation in order to obtain the effect of applying nanoparticles of graphene oxide–silicon carbide on the thermal characteristic. Several nanofluids with different volume concentrations and in a defined temperature range were fabricated, and at last, through fitting curve method, an experimental correlation was developed for determining the thermal conductivity. Esfe et al. [28] experimented the effect of diameter size of the nanoparticles on the convective heat transfer coefficient and also on the pressure drop. TiO_2 /water was considered as the working fluid. In addition, the experimental data were used to develop an artificial neural network (ANN) model to forecast the thermal performance of the selected nanofluid. Karimipour et al. [29] compared the ability of support vector regression (SVR) and ANN to predict conductivity of MWCNT–CuO/water hybrid nanofluid. It was shown that SVR is more accurate where small

data sets were available. Alnaqi et al. [30] employed ANN approaches to estimate the influence of utilizing MWCNT/water nanofluid on the thermal specifications. Shahsavar et al. [31] carried out an experimental investigation in order to measure thermal conductivity and viscosity of paraffin- Fe_3O_4 and used the obtained data to develop a correlation for estimating those parameters through ANN. Bahrami et al. [32] employed the ANN technique to obtain the values of dynamic viscosity and shear rates of Fe-CuO/(ethylene glycol + water) nanofluid at different temperatures and concentrations. Esfe et al. [33] analyzed the accuracy of different ANN techniques on estimating the dynamic viscosity of TiO_2/SAE 50 nanofluid. They modeled the dynamic viscosity through several ANN methods. Among the selected approaches, radial base function is expressed as the most accurate ANN model. ANN techniques have been widely applied in several applications for estimating purposes [14]. Ali et al. [34] performed an experimental investigation to obtain the effect of utilizing TiO_2 /water nanofluid on the overall boiling heat transfer rate. They fabricated nanofluids at various concentrations and reported that at a volume concentration of 0.15, the overall boiling heat transfer coefficient was enhanced to 1.38. Nafchi et al. [35] experimented the effects of volume concentration and temperature of $\text{TiO}_2/\text{ZnO}/\text{EG}$ nanofluid on the viscosity. It was monitored that in higher volume concentration the viscosity of the nanofluid was increased, while in higher temperature it was decreased. Ghasemi et al. [36] investigated the effect of applying COOH-MWCNT nanoparticles on the thermal conductivity. They performed experimental and numerical investigations to propose a predictive model for the thermal conductivity. Vafaei et al. [37] presented an optimal model to predict the thermal conductivity of MgOMWCNTs/EG nanofluid as a function of volume concentration and temperature. They reported that their model was able to predict thermal conductivity with a maximum deviation of 0.008. In overall, it was monitored that the heat transfer coefficient can be increased by applying nanofluids instead of conventional base fluids at certain working conditions. In addition, it is monitored that ANN techniques are reliable and also powerful on the prediction of thermal characteristics for different kinds of nanofluids. Yousefi et al. [38] performed an experimental study alongside proposing an ANN model to predict the thermal characteristics of carbon nanotube. Vakili et al. [39] used experimental data and developed a GA-based statistical model to forecast the viscosity of graphene nanoplate nanofluid. The authors assessed their model under different operational conditions such as different working temperatures and various concentrations of the nanofluid. The preciseness of the model was checked through RMSE and R^2 criteria, which was 0.086 and 0.985, respectively. Adio et al. [40] implemented a study on the experimental measurement and development of a statistical model to predict the viscosity of MgO/ethylene glycol nanofluid. The utilized GA and ANFIS model illustrated a good agreement with the extracted data from experimental measurements.

Furthermore, it has been shown that insertion of twisted tapes while nanofluid is applied causes better heat transfer rate. For example, Fakoor-Pakdaman et al. [41] experimentally analyzed the thermophysical features of MWCNTs nanoparticles in a heat transfer oil base fluid at a vertical helically coiled heat exchanger. It was monitored that this specific design of nanofluid and the utilized geometry of tubes caused the improved overall performance index of 6.4. Al-Rashed et al. [42] performed a second law analysis on a microchannel heat exchanger. They utilized $\gamma\text{-AlO}(\text{OH})$ /(water + ethylene glycol) nanofluid and investigated the impact of nanoparticles' shape on entropy generation. It was monitored that the platelet nanoparticles had the highest rate of total entropy generation and the spherical-shaped nanoparticles had the minimum amount of total entropy generation. Alsarraf et al. [43] tested the performance of $\gamma\text{-AlO}(\text{OH})$ nanofluid as a working fluid of a conventional double-pipe heat exchanger under turbulent flow condition and investigated the effects of shape, Reynolds number, and pressure drop on the overall heat transfer rate. Similar to Al-Rashed et al. [42],

it was reported that the platelet and spherical-shaped nanoparticles had the maximum and minimum values of the overall heat transfer rate. In addition, it was monitored that increasing the Reynolds number and concentrations of nanoparticles yielded a higher heat transfer rate and an increase in the pressure drop.

In the present research, the turbulent heat transfer behavior in the constant wall temperature tube fitted with twisted tapes at twist ratio of 2–8 and using CNT nanofluid at volume concentrations of 0.2–1.2% will be evaluated. In addition, experimental results will be employed in an artificial neural network model to propose a new correlation for calculation of influential parameters on the heat transfer rate including the Nusselt number, friction factor, and overall thermal performance of heat exchangers, while nanofluid and twisted tapes are simultaneously used.

2 Experimental procedures and apparatus

2.1 Nanofluid

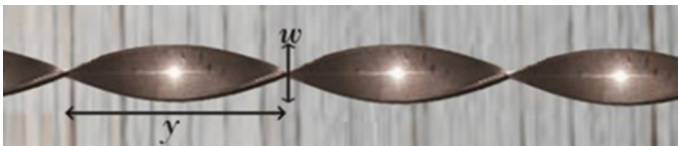
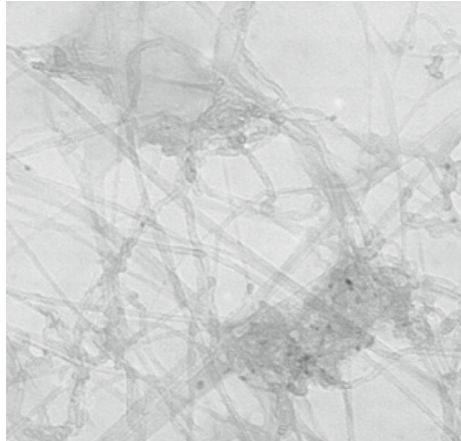
The characterization of the employed CNT nanoparticles is listed in Table 1. Based on the measurements, the outer diameter, the inner diameter, and the average length of the fabricated CNT nanoparticles are 3 nm, 1.2 nm, and 10 nm, respectively. Analyses illustrate that the purity index is 0.95. Moreover, thermophysical properties such as density, thermal conductivity, and specific heat capacity are measured and reported in Table 1. In addition, structural analyses are examined through TEM and the result is illustrated in Fig. 1. The significant step in the fabrication process of the CNT nanofluid is the dispersing process. Dispersing process of CNTs is very crucial since CNTs have a high aspect ratio and large specific surface area. In this research, an effective one-step procedure is carried out by the utilization of potassium persulfate (KPS) as an oxidant to fabricate water-soluble CNT.

2.2 Twisted tape

The utilized twisted tapes are fabricated from aluminum sheet with tape thickness (d), width (w), and length (l) of 0.8 mm, 20 mm, and 800 mm, respectively. In order to prevent extra friction due to insertion of thicker tapes, the thickness of 0.8 mm is selected. Twisted tapes with various twist ratios (y/W) in the range of 2:8 are selected and tested in the experiments. Flat aluminum sheets are twisted with twist length (y) of 6:320 in order to create the twisted tapes at the desired twist ratios ($TR = \frac{Y}{W}$). The geometry of the fabricated tapes is illustrated in Fig. 2.

Table 1 Characterization of CNT

Outer diameter	3 nm
Inner diameter	1.2 nm
Average length	10
Purity	95%
Density (kg/m^3)	1400
Thermal conductivity (W/m K)	3500
Specific heat capacity ($\text{J/kg } ^\circ\text{C}$)	1380

Fig. 1 TEM image of SWCNT**Fig. 2** Illustration of a fabricated twisted tape [44]

2.3 Experimental setup

An open-loop layout is designed and used for the experiments as demonstrated in Fig. 3. The circulation working fluid of this process is CNT nanofluid. A horizontal copper-made tube with the geometry of 3 mm thickness, 22 mm diameter, and 1500 mm length is employed as the heating test tube. The test tube is kept warm through the heat which is provided by an electrical wire heater to have a uniform heat flux distribution. In total, ten thermocouples, *K*-type, are placed on the tube wall. Proper insulation is used to cover the tube and thermocouples in order to reduce heat loss. A rotameter is placed at the inlet of the test tube to measure the flow rate. The flow rate is varied to evaluate the experiments under various Reynolds numbers ($4000 < Re < 20,000$).

A storage tank in a specific height is designed. The working fluid is pumped to the tank and then is entered into the test tube under the natural head. A Variac transformer is provided to regulate the heat flux distribution at the wall of the test tube. At each flux, the system is permitted to obtain steady-state condition at each Reynolds number. Twisted tapes are placed in a distance of 1200 mm from each other. Here, twisted tapes are employed as a swirl generator to provide turbulent flow. The intensity of the turbulence condition is dependent on the selected twist ratios ($y/w = 2, 3, 4, \text{ and } 5$).

3 Data processing

The crucial factors for measuring the heat transfer qualities of nanofluid are its thermophysical specifications [45]. Measurement of thermal conductivity is more difficult than that of other

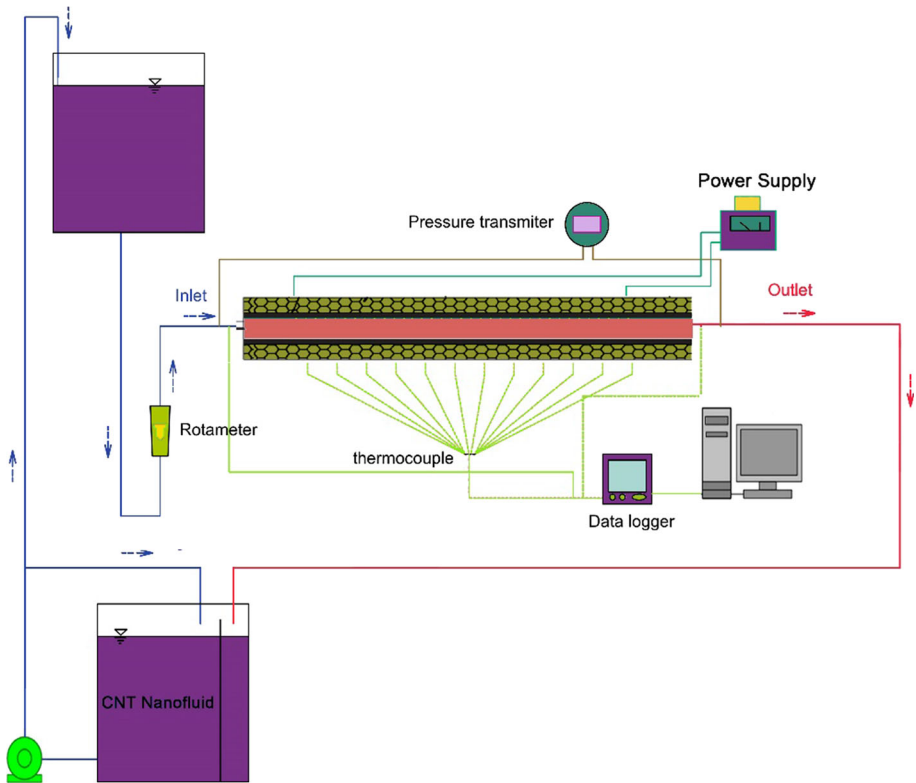


Fig. 3 Representation layout of the experimental setup

thermophysical specifications since outsized errors are associated [46]. The correlation of the nanofluids’ density is:

$$\rho_{nf} = \varphi\rho_{np} + (1 - \varphi)\rho_{bf} \tag{1}$$

The mathematical model about the specific heat value is:

$$(\rho Cp)_{nf} = \varphi(\rho Cp)_{np} + (1 - \varphi)(\rho Cp)_{bf} \tag{2}$$

A KD2 Pro thermal property analyzer is used to measure thermal conductivity. The obtained outcomes at volume concentrations of 0.2% are checked with the Hamilton and Crosser correlation [47] in order to validate the analyzer device:

$$k_{nf} = \frac{k_{np} + (n - 1)k_{bf} + (n - 1)\varphi(k_{np} - k_{bf})}{k_{np} + (n - 1)k_{bf} - \varphi(k_{np} - k_{bf})} k_{bf} \tag{3}$$

To measure the viscosity of the tested nanofluids, Brookfield cone and plate viscometer (LVDV-I PRIME C/P) designed by Brookfield engineering laboratories of USA are utilized. Between the existed theoretical correlations, Khanafer and Vafai’s equation [48] is used to validate the obtained results of the viscosity values:

$$\mu_{nf} = (1.0538 + 0.144\varphi - 3.363 \times 10^{-3}T)\mu_{bf} \tag{4}$$

4 Artificial neural network (ANN)

Back-propagation (BP) approach is an optimization technique which made minimum the target function by adjusting the preliminary weights and biases. Selection of initial weights is a significant step in order to prevent the algorithm from finishing and stopping in the wrong local minimum. In order to surmount this limitation, a stochastic optimization method is added to the BP networks to calculate the optimum values of the network weights. Novel empirical stochastic algorithms have been widely employed for optimization purposes due to their high computational efficiency. It should be noted that an algorithm which achieves the best fit to the data must be chosen. Therefore, genetic algorithm (GA) which has an appropriate performance and demonstrates acceptable results in optimization processes is selected for this study.

The major goal in regulating the weights is to make minimum the target function. This process is usually demonstrated in the words of mean square error (MSE) and R -squared (R^2) which are defined as follows:

$$\text{MSE} = 1/N \sum_{i=1}^N (X_i^{\text{Sim}} - X_i^{\text{ANN}})^2 \quad (5)$$

$$R^2 = \frac{\sum_{i=1}^N (X_i^{\text{Sim}} - \bar{X})^2 - \sum_{i=1}^N (X_i^{\text{Sim}} - X_i^{\text{ANN}})^2}{(X_i^{\text{Sim}} - \bar{X})^2} \quad (6)$$

where N represents the number of data, X_i^{Sim} indicates the obtained value from simulation or measurement, X_i^{ANN} is the value which is calculated by ANN, and the average value is denoted by \bar{X} . The important rules, which are employed to renew the population of chromosomes, are the selection, crossover, and mutation operators. Based on the literature, lower mutation rate and higher crossing over are desired. Mutation is performed as a progressively rise or drop with specific step size producing a new value within the minimum and maximum ranges.

5 Genetic algorithm

GA is a powerful evolutionary technique which is widely employed in energy applications with the aim of system's optimization [49, 50]. This technique is grounded on the survival theory of Darwin and is regulated based on genetic and natural selection [51]. GA has three basic operators as follows:

- Reproduction: employed for choosing the desirable one among a certain population.
- Crossover: to create new individual through conveying characteristics among the mating pool entities.
- Mutation: employed to changeover some of the characteristics of the entities in a random procedure.

The GA drives optimization process built on a random population. Then, the above-mentioned operators are taken apart to function the chosen population so as to breed a new set of data. Next, the generated sets of data (population) are re-assessed to attain the fitness values and also monitored for convergence criterion. In GA, each cycle is defined as generation including the mentioned three basic operators (reproduction, crossover, and mutation) in addition to the evaluation of fitness values.

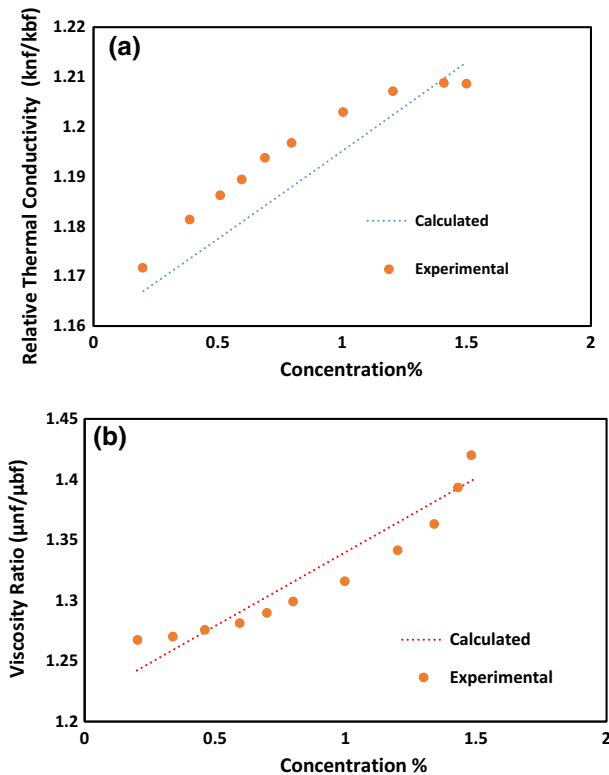


Fig. 4 Thermal conductivity (a) and viscosity (b) of nanofluid versus concentration

6 Results and discussion

6.1 Thermal parameters

Figure 4 demonstrates the result of thermal conductivity (Fig. 4a) and viscosity (Fig. 4b) of fabricated nanofluids in various concentrations at 25 °C. It is monitored that in higher concentrations of nanofluid, higher thermal conductivity and also higher viscosity are obtained in comparison with the base fluid. The maximum value of thermal conductivity, i.e., 1.21 W/m K, is obtained at volume concentration of 1.5%. The outcomes indicate an acceptable convergence with recognized correlations.

6.2 Validation test with water and twisted tapes

Experiments are carried out with water as the working fluid in vacant tubes over the designed Reynolds number in turbulent condition to check the verification and creditability of the procedure. The calculated results are compared and monitored with those results which were obtained by Dittus and Boelter correlation [52] for water to evaluate their correctness:

$$Nu = 0.04Re^{0.75}Pr^{0.4} \quad (7)$$

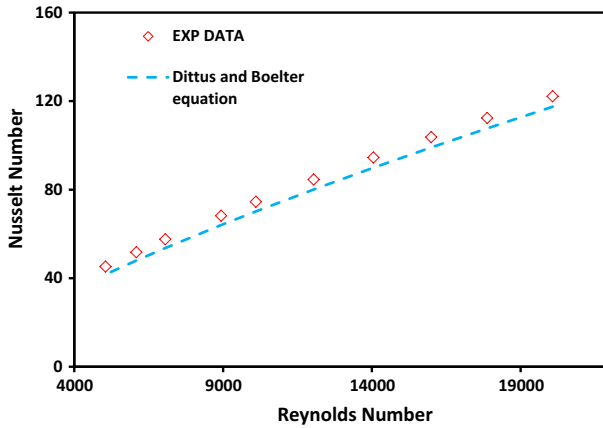


Fig. 5 Nusselt number calculation for simple tube under various Reynolds number: experiments versus Dittus–Boelter equation

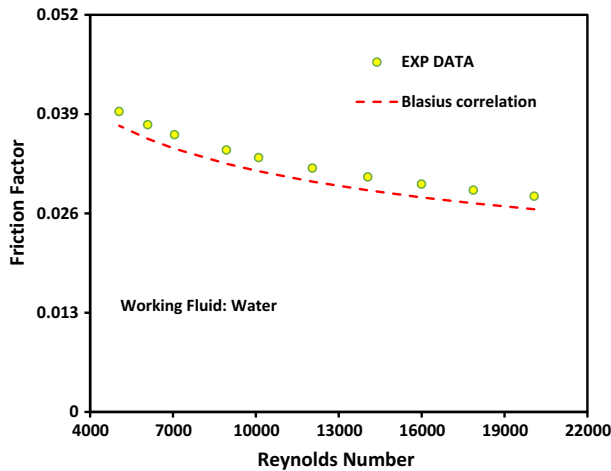


Fig. 6 Friction factor calculation for simple tube under various Reynolds number: experiments versus Blasius correlation

Blasius equation [52] for water is used to compute the friction factor:

$$f = 0.316Re^{-0.25} \tag{8}$$

The Nusselt number and friction factor are measured and compared to those results from Dittus and Boelter correlation and Blasius correlation under the turbulent condition and the outcomes are illustrated in Figs. 5 and 6, respectively. As it is monitored from the figures, measured results from the experimental setup have a reasonable consensus with correlations. The highest Nusselt number of 120 is obtained at Reynolds number higher than 20,000. On the other hand, the lowest friction factor is yielded at Reynolds number of 20,000 by 0.026. The differences for Nusselt number and friction factor of empty water between experiments and correlations are 6% and 2.7%, respectively.

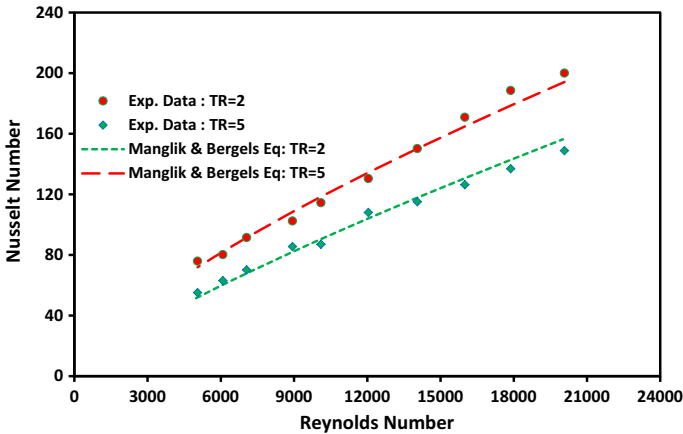


Fig. 7 Nusselt number calculation under various Reynolds number: experiments versus Manglik and Bergles equation

In order to verify the obtained results while the twisted tape is inserted, Manglik and Bergles correlation [23] is used to calculate the Nusselt number and friction factor:

$$Nu = \left(1 + \frac{0.769}{\left(\frac{y}{w}\right)} \right) \left[0.023Re^{0.8}Pr^{0.4} \left(\frac{\pi}{\pi - \left(\frac{4\delta}{d_i}\right)} \right)^{0.8} \left(\frac{\pi + 2 - \left(\frac{2\delta}{d_i}\right)}{\pi - \left(\frac{4\delta}{d_i}\right)} \right)^{0.2} \right] \tag{9}$$

$$f = \left(1 + 2.06 \left(1 + \left(2 \frac{y}{\pi} \right)^2 \right)^{-0.74} \right) * \left[0.079Re^{-0.25} \left(\frac{\pi}{\pi - \left(\frac{4\delta}{d_i}\right)} \right)^{1.75} \left(\frac{\pi + 2 - \left(\frac{2\delta}{d_i}\right)}{\pi - \left(\frac{4\delta}{d_i}\right)} \right)^{1.25} \right] \tag{10}$$

The correctness of the experiments is checked between measured data and results from Manglik and Bergles correlation, and the results are illustrated in Figs. 7 and 8, for Nusselt number and friction factor, respectively. It is monitored that the differences between experiments and correlation are 4.6% for the Nusselt calculation and 1.3% for friction factor. The highest Nusselt number, 200, is obtained at twist ratio of 2 and Reynolds number of 21,000. Increasing the twist ratio decreases the friction factor, and the lowest friction factor is obtained at Reynolds number of 21,000 and twist ratio of 8 about 0.04.

The variation of Nusselt number with Reynolds number is shown in Fig. 9. For all cases, Nusselt numbers considerably increase with increasing Reynolds number. The improvement in heat transfer with increasing Reynolds number is a result of a decrease in thermal boundary thickness.

Due to the creation of swirl flow, when the twisted tape is inserted, heat transfer performance is increased in comparison with the case without twisted tape. In addition, due to the intensification of swirl flow at lower twist ratios, considerable augmentation is monitored in the calculation of the Nusselt number. Moreover, utilization of twisted tapes increases the heat transfer area as a result of increasing the contact surfaces between wall and fluid.

As it was proved in the literature, applying nanofluid enlarges the Nusselt number in comparison with the simple base fluid under certain conditions, and it is boosted up by increasing the nanofluid concentration. In overall, following outcomes are resulted by applying nanofluid: (1) improving the thermal conductivity, heat transfer enhancement as a result

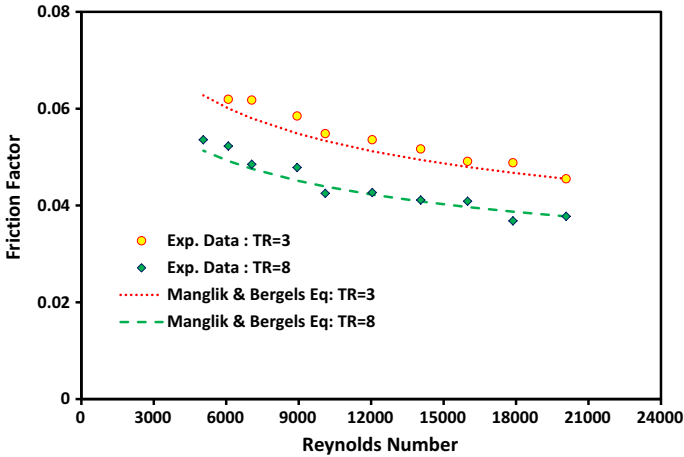


Fig. 8 Friction factor calculation under various Reynolds number: experiments versus Manglik and Bergles equation

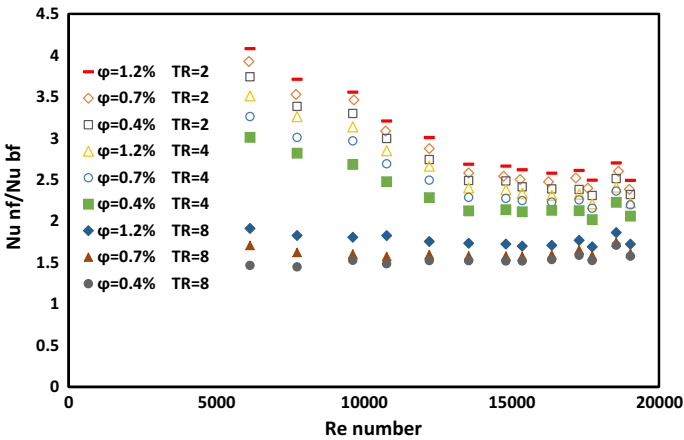


Fig. 9 Nu variation under different conditions of Re number, ϕ , and TR

of nanoparticles' collision; (2) increasing the viscosity of the fluid which has a negative effect on the fluid flow and also on the heat transfer performance. It is monitored from the experiments that positive effect of applying nanofluid on the thermal conductivity is superior to its negative impact on increasing the viscosity.

Visual observations from experiments demonstrate that twisted tapes have a higher influence on the heat transfer enhancement in comparison with the effect of nanofluid on the heat transfer performance. Moreover, the simultaneous application of twisted tapes and nanofluids leads to higher Nusselt number in comparison with the cases where either twisted tape or nanofluid is applied.

The effects of twisted tape and nanofluid concentration on the friction factor are shown in Fig. 10. It is monitored that raising the Reynolds number significantly decreases the friction factor. Applying nanofluids under designed volume concentrations boosts up the friction factor in comparison with the simple base fluid. Moreover, a simultaneous increase

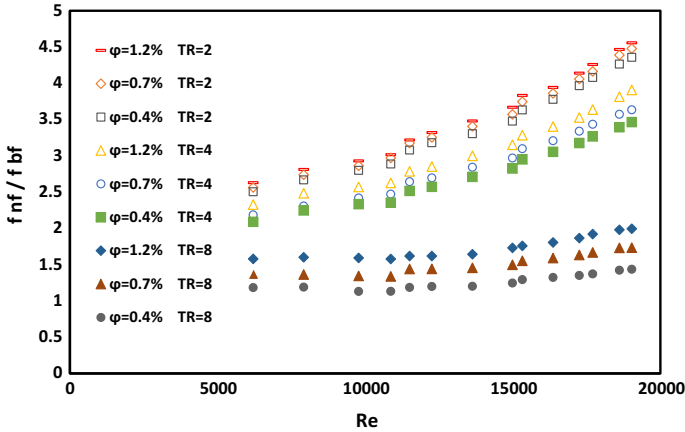


Fig. 10 Factor variation under different conditions of Re number, φ , and TR

in CNT concentration and a decrease in twist ratio lead to increasing the friction factor due to larger shear forces on tube wall as a result of smaller twist ratio or greater concentrations of nanoparticles.

6.3 Thermal performance

In order to evaluate the advantage of utilized application, i.e., nanofluids and twisted tapes, at a constant pumping work, Eq. (11) is used. Therefore, an equality correlation between the pressure drop and the volumetric flow of the enhanced case and the simple case is written as follows:

$$(\dot{V} \Delta P)_E = (\dot{V} \Delta P)_{NE} \tag{11}$$

Equation (11) can also be written in the following form by performing thermodynamic and fluid mechanic regulations to convert volumetric flow and pressure drop into the Reynolds number and friction factor:

$$(f Re^3)_E = (f Re^3)_{NE} \tag{12}$$

where NE represents the base fluid (not enhanced) and E indicates the enhanced case due to the utilization of nanofluids and twisted tapes.

Influences of applying nanofluid at different volume concentrations and twisted tapes at various twist ratios on the thermal performance are illustrated in Fig. 11. It can be easily seen that higher thermal performance is yielded in higher CNT concentrations and smaller twist ratios. Hence, it can be expressed that the advantage of the designed method on the heat transfer enhancement is superior to the disadvantage as a result of pressure drop.

6.4 GA-ANN model

Data are classified into three subsets of training set, validation set, and test set to implement the introduced ANN method. The defined error function is minimized by utilizing the training sets in the networks [53, 54]. Validation sets monitor the error function and choose the network with the lowest value of error. Various scenarios are defined to gather the required experimental data. These scenarios are variations of volume concentrations (φ),

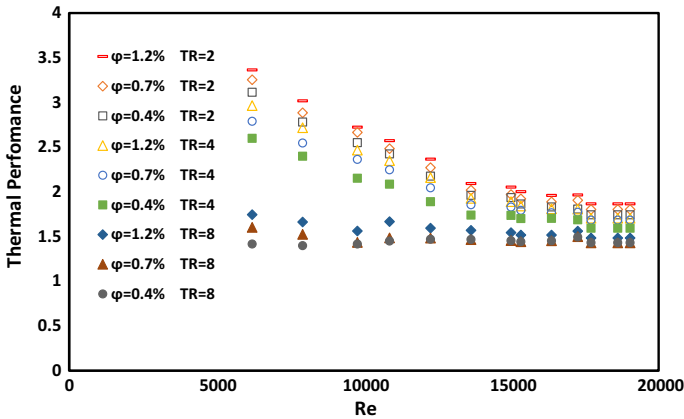


Fig. 11 η variation under different conditions of Re number, ϕ , and TR

Table 2 Outcomes of applied ANN with different configurations

	Neurons in hidden layer	Correlation coefficient	MSE
1	4	0.76	0.034
2	5	0.766	0.046
3	6	0.793	0.095
4	7	0.805	0.080
5	8	0.816	0.088
6	9	0.83	0.051
7	10	0.86	0.017
8	11	0.75	0.036
9	12	0.71	0.047
10	13	0.73	0.49

fabrication of different twist ratios (TR: 2–8), and providing a range for the Reynolds number ($4000 < Re < 20,000$). All input and output data are normalized in order to obtain a better evaluation and judgment.

Specifying the network topology is the first phase toward implementation of the ANN [10, 53]. In order to utilize an approach with the lowest error, a feed-forward artificial neural network with three layers of an input, a hidden, and an output is designed. The next important phase is to determine the optimal neurons' number in different layers. The number of input and output data specifies the neurons' number in the input and output layers, respectively. In order to obtain an optimum number of neurons in the hidden layer, the trial-and-error technique is utilized. Therefore, the training process is performed on a number of networks. The selection of the optimal network is dependent on the maximization of the target function and enhances the network's generalization potential.

It is monitored from Table 2 that a network with ten neurons in the hidden layer yields the most accurate prediction and the minimum value of MSE by 0.017 and the highest correlation coefficient of 0.86. The network arrangement will be yielded in terms of weights and bias values associated with each layer through training, validation, and testing of created networks.

The target function of exergy efficiency is defined when the established ANN model yields a satisfactory performance and then the optimization process is commenced. The trained

Table 3 Employed variable range of the configured GA

Crossover	R^2	Individual	R^2	Mutation rate	R^2	Generation	R^2
0.05	0.76	0.06	0.62	0.021	0.715	20	0.682
0.09	0.81	0.07	0.68	0.025	0.756	25	0.692
0.13	0.85	0.07	0.73	0.03	0.81	35	0.748
0.15	0.87	0.08	0.8	0.036	0.915	45	0.78
0.17	0.89	0.09	0.84	0.04	0.896	55	0.837
0.2	0.91	0.11	0.89	0.048	0.87	65	0.866
0.25	0.84	0.12	0.903	0.053	0.837	75	0.894
0.3	0.77	0.13	0.88	0.06	0.804	85	0.925
0.34	0.74	0.13	0.85	0.075	0.754	95	0.956
0.43	0.72	0.14	0.79	0.08	0.725	105	0.956
0.5	0.62	0.14	0.72	0.505	0.625	115	0.956

networks with GA are employed as the fundamentals to succeed in this stage. The foremost target of the optimization process is to maximize the fitness values, i.e., make minimum the overall MSE. The minimization process is defined as the regulation and optimization of networks' weights. In order to implement the introduced algorithm, a sensitivity analysis is performed to achieve the optimal layout of the presented genetic algorithm. In the initial phase, the mutation rate of 0.02, a crossover rate of 0.5, and an individual number of 0.06 in the early population are set. The selection rule is roulette, the mutation rule is uniform, and the heuristic approach is chosen as the crossover. The genetic population number is regulated to 120. The variables employed in the configuration of the GA are listed in Table 3. It is monitored that the optimal GA configuration has individuals of 0.12, the mutation rate of 0.036, and the crossover rate of 0.2 in the basic population. At last, the response of the implemented technique for a set of input is monitored to yield the optimized genetic algorithm. It can be seen from Table 3 that a selection of 85 generations yields the optimal value of the R -squared statistical index for the GA-ANN. The bold values in Table 3 are representing the final selected results.

In overall, the exergy efficiency with R -squared of $R^2 = 0.9259$ is obtained after implementation of the ANN-GA method.

For the employed BP training approach, the momentum correction factor of 0.7 and the learning coefficient of 0.001 are regulated. GA-ANN is a time-consuming approach. But comparing the ability in error minimization and computation time states that this method is still beneficial. To increase the computation speed led to cut the computation time of the model, local probing terms are employed at the final stage of the algorithm when the overall MSE is minimized or the fitness function is nearly maximized.

The simulated and predicted values of exergy efficiency are graphically compared in Fig. 12. The MSE and coefficient of determination are obtained. It can be seen from Fig. 12 that predicted values demonstrate a satisfactory deviation with the actual measured data. The computation time of 340 s is recorded and demonstrates the powerfulness of the employed model. It is demonstrated in Fig. 12 that the outcomes of the GA-ANN technique are placed in the vicinity of the $X = Y$ line. This closeness illustrates the high level of model accurateness in the exergy efficiency calculation. It can be differently stated that when the predicted output and the real output are similar, they will be located in the slope line of 45° ($X = Y$).

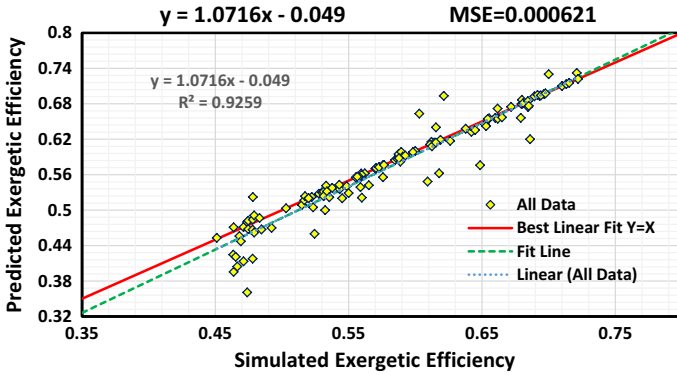


Fig. 12 Scatter plot for exergy efficiency based on GA-ANN method and the R -squared of 0.9259

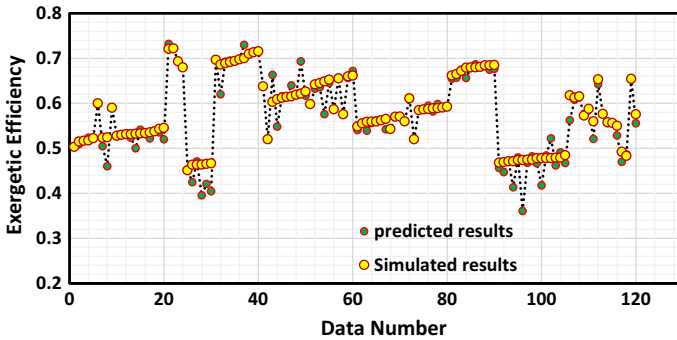


Fig. 13 Comparison of ANN-GA predicted outcomes and experiment values of exergy efficiency for all data

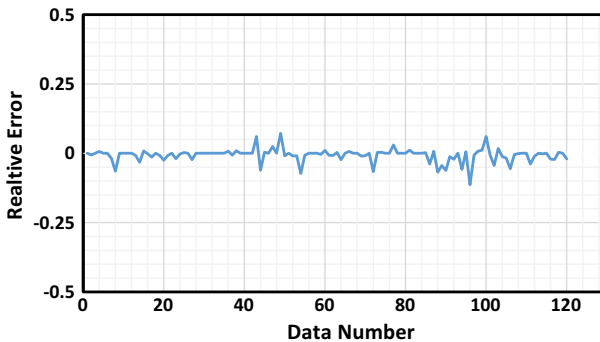


Fig. 14 Relative error between predicted data via neural network and experimental data

This statistical index is known as the correlation coefficient. The correlation coefficient of 1 demonstrates the high precision of the proposed approach. An index number is donated to each data, and the measured exergy efficiency is compared to the predicted exergy efficiency in Fig. 13. It can be monitored from Fig. 13 that the obtained values of the model are close to the real measured values, and this indicates the satisfactory precision of the proposed model. Error diagram shown in Fig. 14 illustrates the closeness of predicted values and real results that it can additionally prove accurate performance of purposed approach.

7 Conclusion

In this investigation, application of CNT/water nanofluid and twisted tape insertion is assessed in a heat exchanger with a fixed wall temperature. Combination of GA and BP for the training phase in the NN algorithm is employed to assess the total exergy performance of the heat exchanger. Following deductions can be obtained from this study:

1. Simultaneous application of nanofluid and twisted tape increases the convective heat transfer, friction factor, and in overall the thermal performance factor.
2. Increasing the CNT volume concentrations and decreasing the twist ratios of the twisted tape yield higher friction factor and convection coefficient and in overall yield improvement in the thermal performance factor.
3. The highest performance factor of 3.4 is yielded when the CNT is applied at the concentration of 1.2%, and twisted tapes are fabricated at the twist ratio of 2.
4. The outcomes based on the presence of nanoparticles demonstrate that the influence of increasing thermal conductivity is superior to the rise of viscosity.
5. The ANN–GA model demonstrated its high accuracy in the prediction of exergy efficiency of the heat exchangers.

Acknowledgements This work is supported by the National Natural Science Foundation of China (Grant No. 51779262). The authors wish to thank the reviewers for their careful, unbiased, and constructive suggestions, which led to this revised manuscript.

References

1. H. Maddah, M. Ghazvini, M.H. Ahmadi, Predicting the efficiency of CuO/water nanofluid in heat pipe heat exchanger using neural network. *Int. Commun. Heat Mass Transf.* **104**, 33–40 (2019). <https://doi.org/10.1016/j.icheatmasstransfer.2019.02.002>
2. M.H. Ahmadi, M. Sadeghzadeh, A.H. Raffiee, K. Chau, Applying GMDH neural network to estimate the thermal resistance and thermal conductivity of pulsating heat pipes. *Eng. Appl. Comput. Fluid Mech.* **13**, 327–336 (2019). <https://doi.org/10.1080/19942060.2019.1582109>
3. S. Eiamsa-ard, P. Promvonge, Performance assessment in a heat exchanger tube with alternate clockwise and counter-clockwise twisted-tape inserts. *Int. J. Heat Mass Transf.* **53**, 1364–1372 (2010). <https://doi.org/10.1016/j.ijheatmasstransfer.2009.12.023>
4. M. Kahani, M.H. Ahmadi, A. Tatar, M. Sadeghzadeh, Development of multilayer perceptron artificial neural network (MLP-ANN) and least square support vector machine (LSSVM) models to predict Nusselt number and pressure drop of TiO₂/water nanofluid flows through non-straight pathways. *Numer. Heat Transf. Part A Appl.* **74**, 1190–1206 (2018). <https://doi.org/10.1080/10407782.2018.1523597>
5. M. Sadeghzadeh, M.H. Ahmadi, M. Kahani, H. Sakhaeinia, H. Chaji, L. Chen, Smart modeling by using artificial intelligence techniques on thermal performance of flat-plate solar collector using nanofluid. *Energy Sci. Eng.* (2019). <https://doi.org/10.1002/ese3.381>
6. N.A.C. Sidik, M.N.A.W.M. Yazid, S. Samion, A review on the use of carbon nanotubes nanofluid for energy harvesting system. *Int. J. Heat Mass Transf.* **111**, 782–794 (2017). <https://doi.org/10.1016/j.ijheatmasstransfer.2017.04.047>
7. S. Qiu, Z. Xie, L. Chen, A. Yang, J. Zhou, Entropy generation analysis for convective heat transfer of nanofluids in tree-shaped network flowing channels. *Therm. Sci. Eng. Prog.* **5**, 546–554 (2018). <https://doi.org/10.1016/j.tsep.2018.02.008>
8. M. Ramezanizadeh, M. Alhuyi Nazari, M.H. Ahmadi, E. Açıkkalp, Application of nanofluids in thermosyphons: a review. *J. Mol. Liq.* **272**, 395–402 (2018). <https://doi.org/10.1016/j.molliq.2018.09.101>
9. M.H. Ahmadi, M. Ghazvini, M. Sadeghzadeh, M. Alhuyi Nazari, M. Ghalandari, Utilization of hybrid nanofluids in solar energy applications: a review. *Nano Struct. Nano Objects* **20**, 100386 (2019). <https://doi.org/10.1016/j.nanoso.2019.100386>
10. H. Maddah, R. Aghayari, M. Mirzaee, M.H. Ahmadi, M. Sadeghzadeh, A.J. Chamkha, Factorial experimental design for the thermal performance of a double pipe heat exchanger using Al₂O₃–TiO₂

- hybrid nanofluid. *Int. Commun. Heat Mass Transf.* **97**, 92–102 (2018). <https://doi.org/10.1016/j.icheatmasstransfer.2018.07.002>
11. A. Baghban, M. Kahani, M.A. Nazari, M.H. Ahmadi, W.-M. Yan, Sensitivity analysis and application of machine learning methods to predict the heat transfer performance of CNT/water nanofluid flows through coils. *Int. J. Heat Mass Transf.* **128**, 825–835 (2019). <https://doi.org/10.1016/j.ijheatmasstransfer.2018.09.041>
 12. M. Ramezanizadeh, M.A. Ahmadi, M.H. Ahmadi, M. Alhuyi Nazari, Rigorous smart model for predicting dynamic viscosity of Al_2O_3 /water nanofluid. *J. Therm. Anal. Calorim.* **137**, 307–316 (2019). <https://doi.org/10.1007/s10973-018-7916-1>
 13. M. Ramezanizadeh, M.H. Ahmadi, M.A. Nazari, M. Sadeghzadeh, L. Chen, A review on the utilized machine learning approaches for modeling the dynamic viscosity of nanofluids. *Renew. Sustain. Energy Rev.* **114**, 109345 (2019). <https://doi.org/10.1016/j.rser.2019.109345>
 14. B. Ruhani, P. Barnoon, D. Toghraie, Statistical investigation for developing a new model for rheological behavior of Silica-ethylene glycol/Water hybrid Newtonian nanofluid using experimental data. *Phys. A Stat. Mech. Appl.* (2019). <https://doi.org/10.1016/j.physa.2019.03.119>
 15. J.A. Eastman, S.U.S. Choi, S. Li, W. Yu, L.J. Thompson, Anomalously increased effective thermal conductivities of ethylene glycol-based nanofluids containing copper nanoparticles. *Appl. Phys. Lett.* **78**, 718–720 (2001). <https://doi.org/10.1063/1.1341218>
 16. A. Ghadimi, R. Saidur, H.S.C. Metselaar, A review of nanofluid stability properties and characterization in stationary conditions. *Int. J. Heat Mass Transf.* **54**, 4051–4068 (2011). <https://doi.org/10.1016/j.ijheatmasstransfer.2011.04.014>
 17. W. Yu, H. Xie, Y. Li, L. Chen, Q. Wang, Experimental investigation on the thermal transport properties of ethylene glycol based nanofluids containing low volume concentration diamond nanoparticles. *Colloids Surf. A Physicochem. Eng. Asp.* **380**, 1–5 (2011). <https://doi.org/10.1016/j.colsurfa.2010.11.020>
 18. D. Wen, Y. Ding, Experimental investigation into convective heat transfer of nanofluids at the entrance region under laminar flow conditions. *Int. J. Heat Mass Transf.* **47**, 5181–5188 (2004). <https://doi.org/10.1016/j.ijheatmasstransfer.2004.07.012>
 19. Y. Yang, Z.G. Zhang, E.A. Grulke, W.B. Anderson, G. Wu, Heat transfer properties of nanoparticle-in-fluid dispersions (nanofluids) in laminar flow. *Int. J. Heat Mass Transf.* **48**, 1107–1116 (2005). <https://doi.org/10.1016/j.ijheatmasstransfer.2004.09.038>
 20. K.S. Hwang, S.P. Jang, S.U.S. Choi, Flow and convective heat transfer characteristics of water-based Al_2O_3 nanofluids in fully developed laminar flow regime. *Int. J. Heat Mass Transf.* **52**, 193–199 (2009). <https://doi.org/10.1016/j.ijheatmasstransfer.2008.06.032>
 21. H. Xie, Y. Li, W. Yu, Intriguingly high convective heat transfer enhancement of nanofluid coolants in laminar flows. *Phys. Lett. A* **374**, 2566–2568 (2010). <https://doi.org/10.1016/j.physleta.2010.04.026>
 22. K. Wongcharee, S. Eiamsa-ard, Friction and heat transfer characteristics of laminar swirl flow through the round tubes inserted with alternate clockwise and counter-clockwise twisted-tapes. *Int. Commun. Heat Mass Transf.* **38**, 348–352 (2011). <https://doi.org/10.1016/j.icheatmasstransfer.2010.12.007>
 23. R.M. Manglik, A.E. Bergles, Heat transfer and pressure drop correlations for twisted-tape inserts in isothermal tubes: part II—transition and turbulent flows. *J. Heat Transf.* **115**, 890 (1993). <https://doi.org/10.1115/1.2911384>
 24. P. Naphon, Heat transfer and pressure drop in the horizontal double pipes with and without twisted tape insert. *Int. Commun. Heat Mass Transf.* **33**, 166–175 (2006). <https://doi.org/10.1016/j.icheatmasstransfer.2005.09.007>
 25. L.S. Sundar, K.V. Sharma, Turbulent heat transfer and friction factor of Al_2O_3 Nanofluid in circular tube with twisted tape inserts. *Int. J. Heat Mass Transf.* **53**, 1409–1416 (2010). <https://doi.org/10.1016/j.ijheatmasstransfer.2009.12.016>
 26. S. Suresh, K.P. Venkataraj, P. Selvakumar, M. Chandrasekar, A comparison of thermal characteristics of Al_2O_3 /water and CuO/water nanofluids in transition flow through a straight circular duct fitted with helical screw tape inserts. *Exp. Therm. Fluid Sci.* **39**, 37–44 (2012). <https://doi.org/10.1016/j.expthermflusci.2012.01.004>
 27. A.A. Mahyari, A. Karimipour, M. Afrand, Effects of dispersed added Graphene Oxide–Silicon Carbide nanoparticles to present a statistical formulation for the mixture thermal properties. *Phys. A Stat. Mech. Appl.* **521**, 98–112 (2019). <https://doi.org/10.1016/j.physa.2019.01.035>
 28. M. Hemmat Esfe, A.A. Nadooshan, A. Arshi, A. Alirezaie, Convective heat transfer and pressure drop of aqua based TiO_2 nanofluids at different diameters of nanoparticles: data analysis and modeling with artificial neural network. *Phys. E Low Dimens. Syst. Nanostruct.* **97**, 155–161 (2018). <https://doi.org/10.1016/j.physe.2017.10.002>
 29. A. Karimipour, S.A. Bagherzadeh, A. Taghipour, A. Abdollahi, M.R. Safaei, A novel nonlinear regression model of SVR as a substitute for ANN to predict conductivity of MWCNT-CuO/water hybrid nanofluid

- based on empirical data. *Phys. A Stat. Mech. Appl.* **521**, 89–97 (2019). <https://doi.org/10.1016/j.physa.2019.01.055>
30. A.A. Alnaqi, S. Sayyad Tavoos Hal, A. Aghaei, M. Soltanimehr, M. Afrand, T.K. Nguyen, Predicting the effect of functionalized multi-walled carbon nanotubes on thermal performance factor of water under various Reynolds number using artificial neural network. *Phys. A Stat. Mech. Appl.* **521**, 493–500 (2019). <https://doi.org/10.1016/j.physa.2019.01.057>
 31. A. Shahsavari, S. Khanmohammadi, A. Karimipour, M. Goodarzi, A novel comprehensive experimental study concerned synthesizes and prepare liquid paraffin-Fe₃O₄ mixture to develop models for both thermal conductivity and viscosity: a new approach of GMDH type of neural network. *Int. J. Heat Mass Transf.* **131**, 432–441 (2019). <https://doi.org/10.1016/j.ijheatmasstransfer.2018.11.069>
 32. M. Bahrani, M. Akbari, S.A. Bagherzadeh, A. Karimipour, M. Afrand, M. Goodarzi, Develop 24 dissimilar ANNs by suitable architectures & training algorithms via sensitivity analysis to better statistical presentation: measure MSEs between targets & ANN for Fe–CuO/Eg–Water nanofluid. *Phys. A Stat. Mech. Appl.* **519**, 159–168 (2019). <https://doi.org/10.1016/j.physa.2018.12.031>
 33. M. Hemmat Esfe, A. Tatar, M.R.H. Ahangar, H. Rostamian, A comparison of performance of several artificial intelligence methods for predicting the dynamic viscosity of TiO₂/SAE 50 nano-lubricant. *Phys. E Low Dimens. Syst. Nanostruct.* **96**, 85–93 (2018). <https://doi.org/10.1016/j.physe.2017.08.019>
 34. H.M. Ali, M.M. Generous, F. Ahmad, M. Irfan, Experimental investigation of nucleate pool boiling heat transfer enhancement of TiO₂–water based nanofluids. *Appl. Therm. Eng.* **113**, 1146–1151 (2017). <https://doi.org/10.1016/j.applthermaleng.2016.11.127>
 35. P.M. Nafchi, A. Karimipour, M. Afrand, The evaluation on a new non-Newtonian hybrid mixture composed of TiO₂/ZnO/EG to present a statistical approach of power law for its rheological and thermal properties. *Phys. A Stat. Mech. Appl.* **516**, 1–18 (2019). <https://doi.org/10.1016/j.physa.2018.10.015>
 36. A. Ghasemi, M. Hassani, M. Goodarzi, M. Afrand, S. Manafi, Appraising influence of COOH-MWCNTs on thermal conductivity of antifreeze using curve fitting and neural network. *Phys. A Stat. Mech. Appl.* **514**, 36–45 (2019). <https://doi.org/10.1016/j.physa.2018.09.004>
 37. M. Vafaei, M. Afrand, N. Sina, R. Kalbasi, F. Sourani, H. Teimouri, Evaluation of thermal conductivity of MgO-MWCNTs/EG hybrid nanofluids based on experimental data by selecting optimal artificial neural networks. *Phys. E Low Dimens. Syst. Nanostruct.* **85**, 90–96 (2017). <https://doi.org/10.1016/j.physe.2016.08.020>
 38. F. Yousefi, H. Karimi, S. Mohammadiyan, Viscosity of carbon nanotube suspension using artificial neural networks with principal component analysis. *Heat Mass Transf.* **52**, 2345–2355 (2016). <https://doi.org/10.1007/s00231-015-1745-6>
 39. M. Vakili, S. Khosrojerdi, P. Aghajannezhad, M. Yahyaee, A hybrid artificial neural network-genetic algorithm modeling approach for viscosity estimation of graphene nanoplatelets nanofluid using experimental data. *Int. Commun. Heat Mass Transf.* **82**, 40–48 (2017). <https://doi.org/10.1016/j.icheatmasstransfer.2017.02.003>
 40. S.A. Adio, M. Mehrabi, M. Sharifpur, J.P. Meyer, Experimental investigation and model development for effective viscosity of MgO–ethylene glycol nanofluids by using dimensional analysis, FCM-ANFIS and GA-PNN techniques. *Int. Commun. Heat Mass Transf.* **72**, 71–83 (2016). <https://doi.org/10.1016/j.icheatmasstransfer.2016.01.005>
 41. M. Fakoor-Pakdaman, M.A. Akhavan-Behabadi, P. Razi, An empirical study on the pressure drop characteristics of nanofluid flow inside helically coiled tubes. *Int. J. Therm. Sci.* **65**, 206–213 (2013). <https://doi.org/10.1016/j.ijthermalsci.2012.10.014>
 42. A.A.A. Al-Rashed, R. Ranjbarzadeh, S. Aghakhani, M. Soltanimehr, M. Afrand, T.K. Nguyen, Entropy generation of boehmite alumina nanofluid flow through a minichannel heat exchanger considering nanoparticle shape effect. *Phys. A Stat. Mech. Appl.* **521**, 724–736 (2019). <https://doi.org/10.1016/j.physa.2019.01.106>
 43. J. Alsarraf, A. Moradikazerouni, A. Shahsavari, M. Afrand, H. Salehipour, M.D. Tran, Hydrothermal analysis of turbulent boehmite alumina nanofluid flow with different nanoparticle shapes in a minichannel heat exchanger using two-phase mixture model. *Phys. A Stat. Mech. Appl.* **520**, 275–288 (2019). <https://doi.org/10.1016/j.physa.2019.01.021>
 44. H. Maddah, M. Alizadeh, N. Ghasemi, S.R. Wan Alwi, Experimental study of Al₂O₃/water nanofluid turbulent heat transfer enhancement in the horizontal double pipes fitted with modified twisted tapes. *Int. J. Heat Mass Transf.* **78**, 1042–1054 (2014). <https://doi.org/10.1016/j.ijheatmasstransfer.2014.07.059>
 45. M.H. Ahmadi, M. Sadeghzadeh, H. Maddah, A. Solouk, R. Kumar, K. Chau, Precise smart model for estimating dynamic viscosity of SiO₂/ethylene glycol–water nanofluid. *Eng. Appl. Comput. Fluid Mech.* **13**, 1095–1105 (2019). <https://doi.org/10.1080/19942060.2019.1668303>

46. M.H. Ahmadi, A. Baghban, M. Sadeghzadeh, M. Hadipoor, M. Ghazvini, Evolving connectionist approaches to compute thermal conductivity of TiO₂/water nanofluid. *Phys. A Stat. Mech. Appl.* (2019). <https://doi.org/10.1016/j.physa.2019.122489>
47. R.L. Hamilton, O.K. Crosser, Thermal conductivity of heterogeneous two-component systems. *Ind. Eng. Chem. Fundam.* **1**, 187–191 (1962). <https://doi.org/10.1021/i160003a005>
48. K. Khanafer, K. Vafai, A critical synthesis of thermophysical characteristics of nanofluids. *Int. J. Heat Mass Transf.* **54**, 4410–4428 (2011). <https://doi.org/10.1016/j.ijheatmasstransfer.2011.04.048>
49. G. Xiao, U. Sultan, M. Ni, H. Peng, X. Zhou, S. Wang, Z. Luo, Design optimization with computational fluid dynamic analysis of β -type Stirling engine. *Appl. Therm. Eng.* **113**, 87–102 (2017). <https://doi.org/10.1016/j.applthermaleng.2016.10.063>
50. S. Woon, L. Tong, O. Querin, G. Steven, Effective optimisation of continuum topologies through a multi-GA system. *Comput. Methods Appl. Mech. Eng.* **194**, 3416–3437 (2005). <https://doi.org/10.1016/j.cma.2004.12.025>
51. S.S. Rao, *Engineering Optimization: Theory and Practice*, 4th edn. (Wiley, Hoboken, 2009). <https://doi.org/10.1002/9780470549124>
52. F.P. Incropera, D.P. DeWitt, T.L. Bergman, A.S. Lavine, *Fundamentals of Heat and Mass Transfer* (Wiley, Hoboken, 2007). <https://doi.org/10.1016/j.applthermaleng.2011.03.022>
53. M.H. Rezaei, M. Sadeghzadeh, M. Alhuyi Nazari, M.H. Ahmadi, F.R. Astarai, Applying GMDH artificial neural network in modeling CO₂ emissions in four nordic countries. *Int. J. Low Carbon Technol.* (2018). <https://doi.org/10.1093/ijlct/cty026>
54. M.H. Ahmadi, M.A. Ahmadi, M. Mehrpooya, M.A. Rosen, Using GMDH neural networks to model the power and torque of a stirling engine. *Sustainability* **7**, 2243–2255 (2015). <https://doi.org/10.3390/su7022243>